Molecular Dynamics Simulations of Bromine Clathrate Hydrates†

Daniel P. Schofield and Kenneth D. Jordan*

Department of Chemistry and Center for Molecular and Materials Simulations, University of Pittsburgh, Pittsburgh, Pennsylvania 15260

Received: January 9, 2009; Revised Manuscript Received: February 20, 2009

A polarizable force field that explicitly includes contributions from exchange repulsion, dispersion, charge penetration, and multipole electrostatics was developed to describe the interaction between bromine and water. This force field was combined with a polarizable force field for water and used in molecular dynamics simulations to calculate the relative energetics of three bromine clathrate hydrates. The simulations predict the tetragonal structure (Allen, K. W.; Jeffrey, G. A. *J. Chem. Phys.* **1963**, *38*, 2304) to be the most stable, with the CS-I and CS-II cubic structures being less stable. Although the CS-II species is not the most stable energetically, we argue that it could be formed under conditions of low bromine concentration, in agreement with recent measurements (Goldschleger, I. U.; Kerenskaya, G.; Janda, K. C.; Apkarian, V. A. *J. Phys. Chem. A* **2008**, *112*, 787) that provide evidence for three different bromine hydrate crystal types.

Introduction

Clathrate hydrates are compounds consisting of rare gas atoms or small guest gas molecules encapsulated within a host framework of rigid polyhedral water cages.[1] The polyhedral cages can be labeled according to the numbers of each type of face they possess. For example, a 5^{12} dodecahedral cage contains 12 faces, each with five water molecules hydrogen bonded in pentagonal rings. The most common hydrate structure is the cubic structure I (CS-I) which has two 5^{12} and six $5^{12}6^2$ cages per unit cell. Methane hydrate, which is present in large volumes on the ocean floor and in permafrost, is generally found as a CS-I hydrate.[1] Larger molecules such as propane form a cubic structure II (CS-II) hydrate which has sixteen 5^{12} and eight $5^{12}6^4$ cages per unit cell, with only the large cages being occupied.

In some cases multiple crystalline structures for gas hydrates can be observed. For example, trimethylene oxide (TMO) forms either a CS-I or CS-II hydrate depending on the stoichiometry.[2] At high concentrations of TMO, the CS-I hydrate is formed and at low concentrations of TMO, the CS-II hydrate is formed with only the larger cages occupied in both cases. Crystals of different morphology are also observed for cyclopropane hydrate, with the observed hydrate structures again being CS-I or CS-II depending on the temperature.[3]

In this paper we investigate the stability of three crystal structures of bromine hydrate. The structure of bromine hydrate has long been controversial. Allen and Jeffrey originally proposed a tetragonal unit cell (TS-I).[4] However, as reviewed in ref 5, other authors interpreted the wide range of observed H_2O:Br_2 stoichiometries as indicative of the presence of different hydrate crystals. More recent X-ray diffraction measurements for bromine hydrate crystals of variable stoichiometry formed under different physical conditions indicated that all the crystals had a tetragonal unit cell as suggested by Allen and Jeffrey.[6] This tetragonal unit cell is unique to bromine hydrate and is comprised of ten 5^{12}, sixteen $5^{12}6^2$, and four $5^{12}6^3$ cages. For ease of notation we refer to 5^{12}, $5^{12}6^2$, $5^{12}6^3$, and $5^{12}6^4$ cages as dodecahedral (D), tetrakaidecahedral (T), pentakaidecahedral (P), and hexakaidecahedral (H) cages, respectively.[7] In TS-I bromine hydrate the small D cages are unoccupied and varying occupation of the larger T and P cages is believed to account for the range in stoichiometries observed in previous experiments.[6] Attempts to form a CS-II bromine hydrate with Xe as a helper gas resulted in a metastable crystal.[6] The metastability of the CS-II double hydrate is in agreement with previous composition measurements that have resulted in H_2O:Br_2 stoichiometries ranging from 12:1 to 6:1,[5] values that are far removed from the 17:1 value required for the CS-II structure.

Although the crystallographic work of refs 4 and 6 indicated that bromine hydrate forms only TS-I crystals, recent measurements of the resonance Raman and the electronic absorption spectra of bromine hydrate provide evidence for nontetrahedral crystals.[8,9] In ref 8 it was found that when a TS-I crystal was exposed to excess water at temperatures below 266 K, cubic crystals were formed on the surface of the TS-I crystal.[8] The stretching frequency of the Br_2 molecules in the cubic crystal is lower than that observed in the TS-I structure, which indicates a more favorable interaction between bromine and the hydrate cage in the former. The cubic crystal was attributed to CS-II on the basis that this structure has the large H cage type which allows the greatest flexibility for Br_2 to orient in an energetically favorable configuration. A subsequent study from the same group has also indicated the existence of metastable crystals, which were assigned as CS-I.[9]

In the present work we characterize theoretically the relative stability of the three bromine hydrate crystals as a function of temperature using molecular dynamics simulations with a bromine−water force field derived from the results of ab initio resolution-of-the-identity second-order Moller−Plesset perturbation (RIMP2),[10,11] coupled cluster singles, doubles and perturbative triples (CCSD(T)),[12,13] and reduced variational space (RVS) calculations.[14]

Computational Methods

Force Field Development. To model bromine hydrate, one needs a force field that describes the H_2O-H_2O, H_2O-Br_2, and Br_2-Br_2 interactions. Studies of methane hydrate have shown that simulations with polarizable water models are more

† Part of the "Robert Benny Gerber Festschrift".

* To whom correspondence should be addressed, jordan@pitt.edu.

10.1021/jp900237j CCC: $40.75
Published on Web 03/24/2009

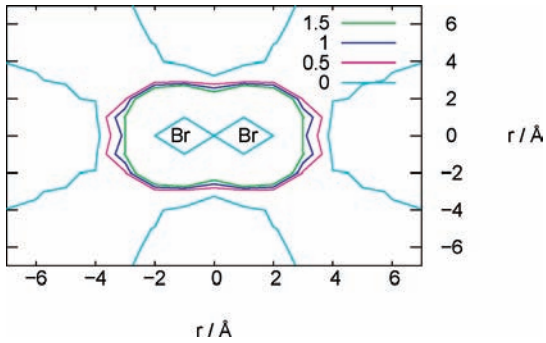

Figure 1. Difference between the electrostatic potential of Br_2 as described by the distributed multipole representation used in our force field and that from CCSD/aug-cc-pVQZ-PP calculations. The contour levels are in kcal mol^{-1}.

successful at reproducing the available experimental data than are simulations with force fields that do not explicitly account for polarization.[15,16] For this reason, we decided to employ a force field that accounts for polarization of both the water and bromine molecules. There are many polarizable water models, and in this work we have adopted the polarizable charge-on-a-spring (COS/G2) water model.[17] This model represents the electrostatics with positive point charges on the hydrogen atoms and a countering negative point charge at an M-site located 0.22 Å from the oxygen atom, displaced toward the H atoms, along the HOH angle bisector. The charge-on-a-spring site is placed at the M-site, and the dispersion and repulsion interactions are represented by a 12-6 Lennard-Jones potential between oxygen atoms.[17]

To the best of our knowledge there is no polarizable force field for bromine in the literature, and we undertook development of such a model in this work. To accomplish this, we carried out ab initio electronic structure calculations on Br_2, employing a pseudopotential[18] for the innermost 10 electrons on each atom together with the aug-cc-pVQZ-PP basis set, developed for use with this pseudopotential.[18] In calculations using the resolution-of-the-identity approximation, all-electrons of Br_2 were treated explicitly. All calculations were performed using the experimental Br−Br bond length of 2.28326 Å.[19]

The first step in the development of the water−bromine force field was to develop a representation of the static charge distribution of Br_2. This was accomplished through use of Stone's distributed multipole analysis (GDMA)[20] to decompose the CCSD/aug-cc-pVQZ-PP electron density into contributions from multipoles centered on the atoms and at the bond midpoint (BM-site). The electrostatic potentials generated using various distributed multipoles were then compared to that from the CCSD/aug-cc-pVQZ-PP calculations. We found it necessary to employ charges (q), dipoles (μ), and quadrupoles (Θ) at the atomic sites and a charge at the BM-site in order to accurately reproduce the ab initio electrostatic potential at distances more than 3 Å from a Br atom as shown in Figure 1. For implementation in the DL_POLY molecular dynamics package,[21] the dipoles and quadrupoles were represented in terms of point charges, rather than as point multipoles. This has a negligible effect on the calculated electrostatic potential at distances relevant for our simulations. The calculations of the CCSD electron density and the associated electrostatic potential were carried out with the Gaussian 03 package.[22]

The polarizability of the bromine molecule is incorporated through use of a single charge-on-a-spring located at the BM-site. The mobile charge is taken to be −8.0 |e|, and the force constant is chosen to reproduce the mean polarizability of Br_2 calculated at the CCSD(T)/aug-cc-pVQZ-PP level. The calculation of the molecular polarizability was carried out with a finite-field approach using the MOLPRO program.[23]

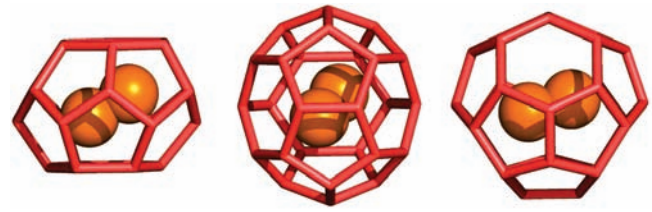

Figure 2. Br_2 encapsulated in $5^{12}6^2$, $5^{12}6^3$, and $5^{12}6^4$ cages. The structures shown are the lowest energy orientations obtained from the scans of the potential energy surfaces.

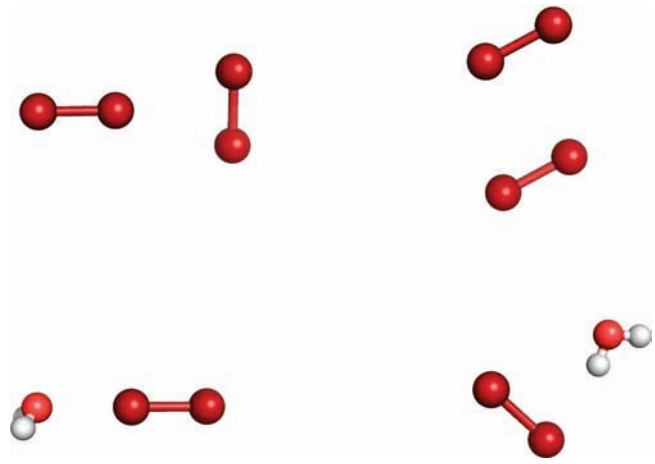

Figure 3. Potential energy minima on the CCSD(T) Br_2−Br_2 (top) and MP2 Br_2−H_2O (bottom) potential energy surfaces.

To determine the force field parameters for the interaction of water and bromine, we carried out ab initio calculations for a Br_2 molecule contained in a T-type cage. The positions of the oxygen atoms for the Br_2−$(H_2O)_{24}$ cluster were taken from the crystal structure of bromine hydrate TS-I,[6] and the hydrogen atoms were positioned as described later. The bromine molecule was placed at the center of the cage, and its orientation about arbitrary polar axes was varied from 0 to 180° in 15° increments. The energy at each orientation was calculated with the RIMP2 method using the aug-cc-pVTZ and cc-pVDZ basis sets on Br_2 and H_2O, respectively. For the lowest energy structure from this two-dimensional scan (Figure 2), the 24 Br_2−H_2O dimers were "cut out", and for each dimer MP2/aug-cc-pVQZ-PP potential energy curves were generated by varying the oxygen to BM-site distance. The potential energy curves were calculated by displacing the water molecules from −1.4 to 1.4 Å relative to their positions in the cage. The grid points were spaced by 0.2 Å increments with two additional points at ±0.1 Å. Potential energy curves were also calculated starting from two local minima for the Br_2−H_2O dimer (see Figure 3). Unless otherwise mentioned, in all ab initio calculations the counterpoise correction[24] was applied to account for basis set superposition error (BSSE).

The interaction energy at each point on each Br_2−H_2O potential energy curve was decomposed using a RVS analysis with the all-electron aug-cc-pVTZ[25] basis set. These calculations separate the Hartree−Fock (HF) interaction energy into contributions from electrostatics, polarization, charge-transfer, and exchange repulsion and were carried out with the GAMESS package.[26] The exchange-repulsion, charge-transfer, and electrostatic contributions from the RVS calculation were used in

TABLE 1: Description of the Br_2-Br_2 and Br_2-H_2O Force Fields

interaction	input data	functional form
electrostatics, H_2O	from ref 17	q on H atoms and M-site
electrostatics, Br_2	GDMA of CCSD/aug-cc-pVQZ-PP electron density	q, μ, and Θ on Br, q' on BM-site
polarization, H_2O	from ref 17	COS at M-site
polarization, Br_2	spherical polarizability from CCSD(T)/aug-cc-pVQZ-PP calculations	COS at BM-site
exchange repulsion	RVS decomposition of HF/aug-cc-pVTZ energies	$A\exp(-r/b)$
dispersion	difference between MP2 (H_2O-Br_2) or CCSD(T) (Br_2-Br_2) and HF interaction energies	$\frac{-C_6}{r^6}\left(1-\left(\sum_{k=0}^{6}\frac{(\delta r)^k}{k!}\right)\exp(-\delta r)\right)$
charge penetration[a]	difference between the electrostatic energies and distributed multipole calculations	$D\exp(-r/f)$
charge transfer[a]	from RVS calculations	

[a] The charge-penetration and charge-transfer energies are combined and used in determining the parameters in the $D\exp(-r/f)$ term.

TABLE 2: Parameters Used in the Br_2-H_2O and Br_2-Br_2 Force Fields

	exchange repulsion		dispersion		charge penetration[a]	
	A (kcal mol^{-1})	b (Å)	C_6 (kcal mol^{-1} Å^6)	δ (Å^{-1})	D (kcal mol^{-1})	f (Å)
O−Br	83660.1	0.303261	1556.38	3.03179	−100167.0	0.278593
H−Br	2208.42	0.389031	202.18	4.74015	−483.61	0.437844
Br−Br	83879.6	0.354679	3891.11	3.32721	−36326.60	0.359058

[a] Also includes the charge-transfer contribution.

the development of our force field as described below and are summarized in Table 1. The exchange-repulsion contribution to the potential is represented as Buckingham[27] type $Ae^{-r/b}$ exponential terms in the interatomic Br−O and Br−H distances, with the parameters being fit to the corresponding RVS results.

At large separation between monomers, the electrostatic interaction is well-represented in terms of the distributed multipole expansions. However, at short distances, where the charge distributions of the monomers overlap, there is also a contribution due to charge penetration.[28,29] We approximate the charge penetration contribution to the interaction energies by the difference between the electrostatic energies calculated with the RVS procedure and those from the multipole expansion. The resulting charge-penetration and RVS charge-transfer energies were combined and fit to exponential terms in the Br−O and Br−H distances. An attempt was made to describe both the charge penetration and the exchange repulsion with single Br−O and Br−H exponentials; however, this proved much less satisfactory than employing two separate exponential terms between each pair of atoms.

The polarization contributions from the RVS calculation were not used in parametrizing the Br_2-H_2O force field as this contribution was assumed to be described by the COS model. The dispersion energies were approximated by the differences between the HF/aug-cc-pVQZ-PP and MP2/aug-cc-pVQZ-PP interaction energies and were fitted to damped C_6/r^6 potentials between the atoms of the monomers. The damping function is that of Tang and Toennies.[30]

The functional forms of the various terms in the force field are given in Table 1. The individual parameters were determined using least-squares fitting and are summarized in Table 2. The decomposition of the energy for one of the 24 dimers is shown in Figure 4.

To determine the parameters for the Br_2-Br_2 interaction potential, ab initio potential energy curves as a function of the BM−BM distance were calculated for Br_2-Br_2 starting from the two local minima shown in Figure 3. The same step size was used as for the Br_2-H_2O dimers. For Br_2-H_2O, MP2 and CCSD(T) calculations give similar interaction energies and, as a result, the MP2 method was adopted to generate the potentials. In contrast, for the Br_2-Br_2 dimers, MP2 calculations give much larger binding energies than do CCSD(T) calculations, indicating an inadequacy of the MP2 method in this case. For this reason the differences between the CCSD(T) and Hartree−Fock energies were used to estimate the dispersion contribution to the Br_2-Br_2 interaction energies.

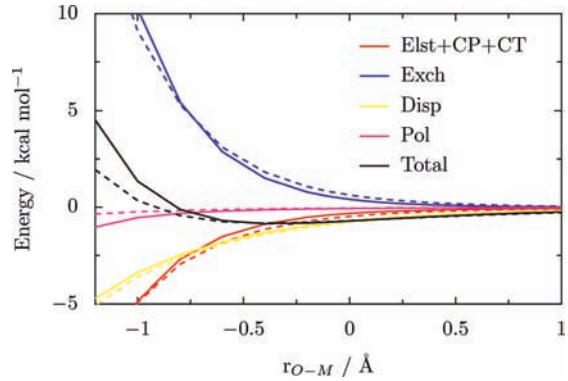

Figure 4. Decomposition of the interaction energy for one of the Br_2-H_2O dimers sampled from a T cage in bromine hydrate. The solid lines correspond to ab initio results and the dashed lines to results obtained with our model potential.

To test the resulting force field parameters for describing the Br_2−water interactions, RIMP2 potential energy surface scans were carried out for $Br_2-(H_2O)_{26}$ and $Br_2-(H_2O)_{28}$ clusters, to model a Br_2 molecule in the type P and H cages, respectively. These calculations were performed using the same basis set as for the T cage. The minimum energy configurations from the potential energy surface scans were then used for single-point RIMP2 and RI-LCCSD(T) calculations with larger basis sets to investigate the dependence of the binding energy upon the basis set and ab initio method employed.

Simulation Details. The potential energies for each of the hydrate structures were obtained from NPT molecular dynamics simulations, carried out with the Nosé-Hoover thermostat and barostat[31,32] and coupling times of 0.2 and 1.0 ps for temperature

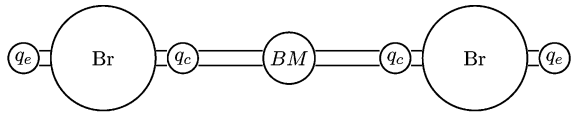

q		1.477		-2.954	1.477	
μ_z	-2.188		2.188	2.188		-2.188
Θ_{zz}	8.698	-17.396	8.698	8.698	-17.396	8.698

Figure 5. Model for the electrostatic interactions of bromine. The compressed (q_c) and extended (q_e) charges are located $0.5a_0$ from the atomic sites and are chosen to give atomic charges (q), dipoles (μ_z), and quadrupoles (Θ_{zz}) of 1.477e, $\pm$2.188ea_0, and 4.349ea_0^2, respectively. The first, second, and third rows of numbers represent the charges required to approximate the atomic charges, dipoles, and quadrupoles, respectively.

and pressure, respectively. Each system was preequilibrated for 100 ps with the Berendsen thermostat and barostat,[33] before being further equilibrated for 10 ps with the Nosé-Hoover thermostat and barostat. Averages were collected from 100 ps production runs. The time step used in the simulations was 1 fs. The intermolecular interactions were cutoff at 11.0 Å, and the long-range electrostatics were accounted for by the particle mesh Ewald method.[34] The water and bromine molecules were constrained to be rigid bodies through use of the NOSQUISH[35] and RATTLE[36] algorithms. The initial positions of the oxygen atoms in the TS-I lattice were taken from the X-ray study of Udachin et al.,[6] with the hydrogen atoms distributed according to the scheme of Buch et al.[37] to produce a unit cell with low dipole moment. For the CS-I hydrate the initial oxygen positions were obtained from the X-ray structure of ethylene oxide hydrate,[38] with protons again disordered to produce a unit cell with low dipole moment.[15] The CS-II hydrate lattice was obtained from the hydrogen hydrate simulations of Alavi et al.[39] For the TS-I hydrate a $1 \times 1 \times 2$ supercell with initial box lengths of 23.0436 Å for the a- and b-axes and 24.149 Å for the c-axis, was employed. For the CS-I and CS-II hydrates we used $2 \times 2 \times 2$ supercells with initial box lengths of 24.06 and 34.0 Å, respectively. For all three hydrates, the small D cages were left empty and the larger cages were fully occupied. For the TS-I crystal the simulation box contained 344 H_2O and 40 Br_2 molecules, for the CS-I crystal it contained 368 H_2O and 48 Br_2 molecules, and for the CS-II crystal it contained 1088 H_2O and 64 Br_2 molecules. The simulations were run at a pressure of 1 atm and over a range of temperatures from 80 to 260 K. These results span the temperature range of previous X-ray diffraction measurements, which were carried out at 173 K[6] and 263 K.[4] The authors of ref 8 observe multiple crystal structures over the temperature range 228−266 K.

Results And Discussion

Br_2−Water Interaction. As noted above, it is necessary to employ moments through the quadrupole on the Br atoms to adequately describe electrostatic interactions involving Br_2. A similar conclusion has been reached by Torii.[40] In order to represent the dipole and quadrupole moments in terms of distributions of point charges, two additional sites positioned $\pm 0.5a_0$ from each bromine atom, along the rotational axis, were introduced. The dipole was then modeled by placing two charges of $\pm q$ on these additional sites. The quadrupole was included by placing charges of $+q'$ on the extra sites and charges of $-2q'$ on the atoms. The distribution of point charges used to represent the various multipoles is shown in Figure 5. The value of the molecular quadrupole of Br_2 as described by the model (3.569 ea_0^2) is, by design, in excellent agreement with the CCSD/aug-cc-pVQZ-PP calculated value of 3.589 and is close to the experimental value of 3.9 ea_0^2.[41]

TABLE 3: Mean Difference between Charge-on-a-Spring (COS) and RIMP2/aug-cc-pVQZ-PP (QM) Calculated Binding Energies (kcal mol^{-1}) for the 24 Br_2−H_2O Dimers from the T-Type Cage[a]

energy component	$E_{COS} - E_{QM}$
electrostatics[b]	−0.137
exchange repulsion	0.166
dispersion	−0.031
polarization	0.067
total	0.076

[a] The errors are determined at the intermolecular distance found in the cage geometry. [b] including charge penetration and charge transfer.

Although the polarizability of Br_2 is quite anisotropic, the near spherical shape of the water cages means that the polarization contributions to the interaction energies are small. The resultant error introduced by the adoption of an isotropic polarizability should be small, and the model potential for Br_2 employs a single isotropic polarizable center located at the BM-site. The model polarizability is the mean value from CCSD(T)/aug-cc-pVQZ-PP calculations, which give values of 9.15 and 5.37 Å^3, respectively, for the parallel and perpendicular components of the polarizability of Br_2.

The parameters determined for the Br_2−H_2O force field are given in Table 2. The errors associated with fitting the dispersion, electrostatics, and exchange are summarized in Table 3. For the 24 Br_2−H_2O dimers that make up the T cage, the binding energies calculated with the model potential differ from the RIMP2/aug-cc-pVQZ-PP values on average by only 0.076 kcal mol^{-1}. Analysis of the individual contributions that comprise the total binding energy shows that at the minimum energy geometry for Br_2 in the cage, our COS model gives too positive a value for the exchange repulsion and too negative a value for the electrostatic interaction, with the two errors almost canceling. As both the exchange repulsion and the charge penetration are fit with the same functional form, this confirms that a Buckingham-type potential is not ideal for describing these two interactions. Previous theoretical studies of liquid bromine and chlorine have used complicated anisotropic potentials to describe the exchange repulsion for these systems.[42−45] It is likely that anistropic functions for the charge penetration and exchange repulsion would improve the quality of the Br_2−H_2O potential; however this is beyond the scope of the present work. From Table 3 it is seen that the polarization energy is slightly underestimated in magnitude for Br_2−H_2O dimers cut out of the T-cage, probably due to the use of a single polarizable site on the monomers and possibly also due to the neglect of the effect of charge penetration on the polarization energies. From Figure 4 it is seen that at short distances between the Br_2 and H_2O molecules, the polarization energy is considerably underestimated; however this region of the potential is unlikely to be sampled in our simulations.

Potential energy surfaces for Br_2 inside the T, P, and H cages are shown in Figure 6. The shapes of the potential energy surfaces calculated with the COS model compare well with those calculated with the RIMP2/aug-cc-pVTZ(Br)-cc-pVDZ(O,H) method; however the magnitudes of the binding energies are much larger with the model potential. This is due primarily to the inadequacy of the aug-cc-pVTZ(Br)-cc-pVDZ(O,H) basis

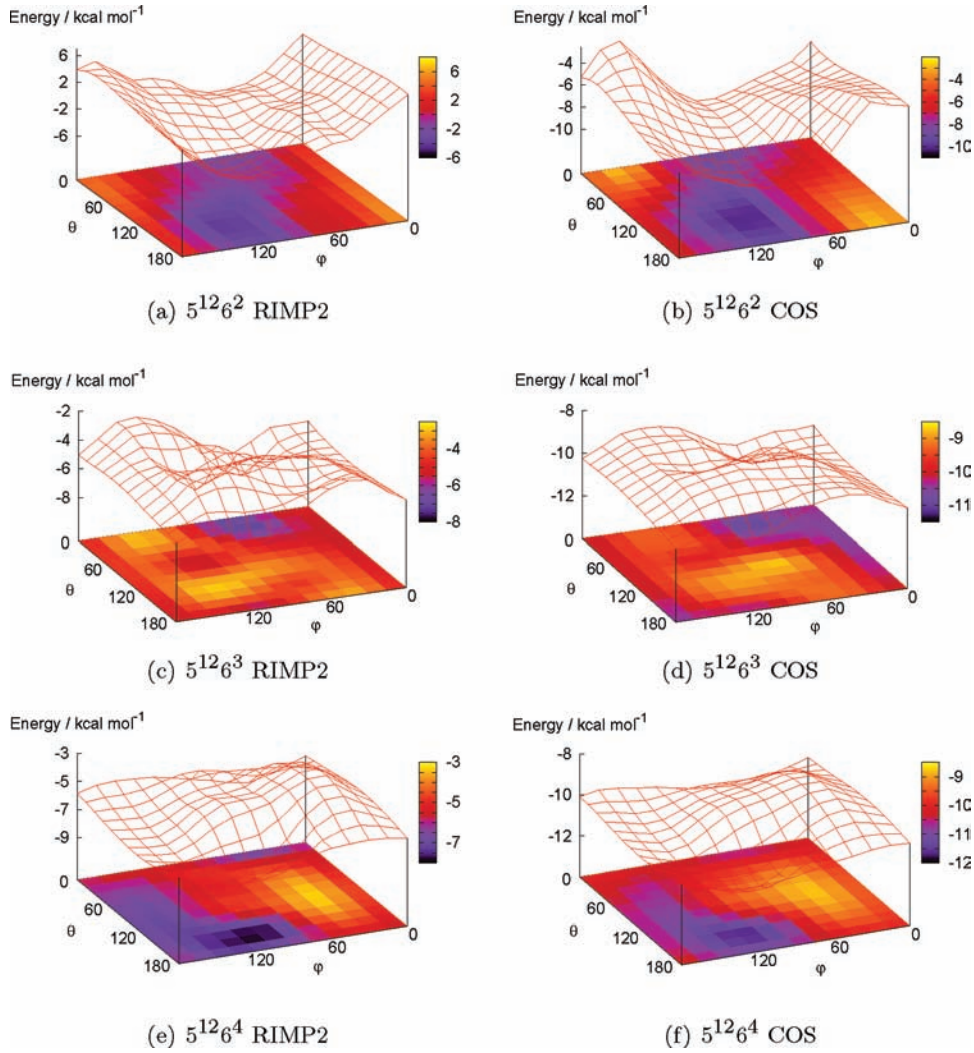

Figure 6. Potential energy surfaces for Br_2 encapsulated in the T, P, and H clathrate cages. The RIMP2 results are obtained using the aug-cc-pVTZ basis set on Br_2 and the cc-pVDZ basis set on water. The COS values are calculated with the model potential developed in this work. ϕ and θ are arbitrarily assigned polar angles.

TABLE 4: Calculated Binding Energy (kcal mol^{-1}) for Placing Br_2 in Different Hydrate Cages

method	basis set[a]			cage type		
	Br	O	H	$5^{12}6^2$	$5^{12}6^3$	$5^{12}6^4$
RIMP2	AVTZ	VDZ	VDZ	−4.1	−7.6	−8.0
RIMP2	AVQZ	AVTZ	VDZ	−9.2	−11.8	−11.8
RIMP2	AVQZ	AVTZ	VTZ	−9.5[b]	−12.1	−12.0
LCCSD(T)	AVQZ	AVTZ	VDZ	−8.0	−10.6	−10.8
MMFF[46]				−1.4	−5.7	−5.0
COS (this work)				−10.0	−11.1	−11.7

[a] AVQZ=aug-cc-pVQZ, AVTZ=aug-cc-pVTZ, VTZ=cc-pVTZ and VDZ=cc-pVDZ [b] In this case the value without the counterpoise correction is 12.1 kcal mol^{-1}.

set used to generate the ab initio potential energy surfaces. As can be seen from Table 4, expanding the basis set from aug-cc-pVTZ(Br)-cc-pVDZ(O,H) to aug-cc-pVQZ(Br)-aug-cc-pVTZ(O)-cc-pVTZ(H) leads to large increases in the magnitudes of the binding energies. Because the potential energy surface scans consist of 145 grid points, RIMP2 calculations for the entire grid with the larger basis set would have been computationally prohibitive. It is likely that the binding energies would be further enhanced by around 1 kcal mol^{-1} in going to the complete basis set limit. However, higher-order correlation effects cause a reduction of the interaction energies of similar magnitude as can be seen from the results of localized orbital CCSD(T)[47,48] calculations, also reported in Table 4.

Table 4 also reports binding energies obtained through use of the Merck molecular force field (MMFF).[46] It is clear that the MMFF model greatly underestimates the interaction between Br_2 and the water cages. In contrast, the COS force field developed in the present study provides interaction energies that are in reasonable agreement with the highest level ab initio values. However, it appears that our COS-type model potential overbinds Br_2 in the T cage by around 1.5 kcal mol^{-1}.

Relative Stability of the Different Hydrates. In order to elucidate the factors responsible for Br_2 forming a unique TS-I hydrate structure, we carried out a series of molecular dynamics simulations using the force field derived in this study. Due to the different H_2O:Br_2 ratios in each of the hydrate structures, it is difficult to obtain relative energies for comparison. To facilitate comparison, we scale the results of our simulations up to a system size of 16813 water molecules. This is the lowest number of water molecules which results in a whole number of bromine molecules for each crystal type. This gives 2193, 989, or 1955 Br_2 molecules for CS-I, CS-II, or TS-I, respectively.

Bromine is the only substance known to form a TS-I hydrate structure. Chlorine forms a CS-I hydrate structure with complete or near complete occupancy of the T cages and partial

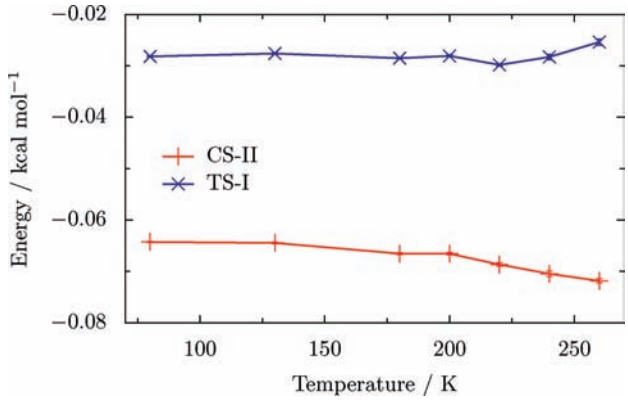

Figure 7. Energies per water molecule of the empty TS-I and CS-II lattices relative to that of the CS-I lattice.

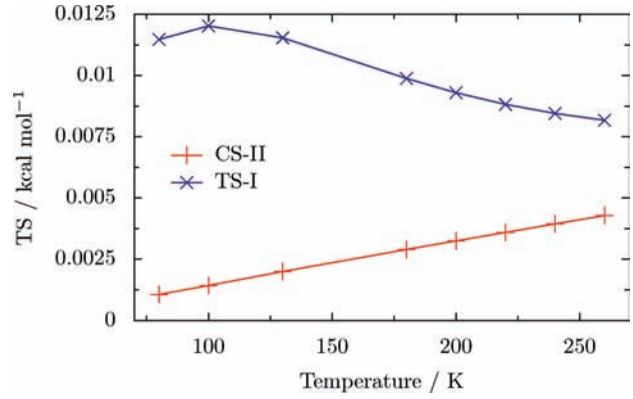

Figure 8. Entropic contribution to the free energy for the empty TS-I and CS-II lattices relative to that of the CS-I lattice.

occupancy of the D cages.[49] It might be expected therefore, that bromine could form a CS-I structure with the D cages completely empty. This postulate is further supported by the similar van der Waals radii of Br_2 (598 pm)[50] and TMO (610 pm),[2] the latter of which forms both CS-I and CS-II hydrates.[2] Upon observation that Br_2 forms a TS-I structure, previous researchers have inferred that the stability of Br_2 in the *P* cage must be markedly greater than that in the T cage.[46] Our highest level ab initio calculations predict that Br_2 is 2.6 kcal mol^{-1} more stable in the P cage than in the T cage, which is not large enough to ovecome the decreased number of Br_2-H_2O interactions in the TS-I hydrate relative to the CS-I hydrate.

The potential energies of the empty CS-II and TS-I lattices relative to that of the empty CS-I lattice are reported in Figure 7. As expected, the CS-II lattice is the most stable, and the CS-I lattice the least stable, consistent with the stability of the empty lattices following the fraction of the cages that are dodecahedral. Per water molecule, we calculate the potential energy difference between the CS-I and CS-II hydrate to be 0.072 kcal mol^{-1} at $T = 260$ K and $P = 1.01325$ bar, which compares reasonably well with the difference of 0.040 kcal mol^{-1} at $T = 273.15$ K and $P = 1$ bar deduced by Handa and Tse[51] from analysis of the thermophysical properties of CS-I Xe hydrate and CS-II Kr hydrate in terms of the model of van der Waals and Platteeuw.[52]

To determine the effect of entropy on the relative stability of the three hydrate lattices, we used lattice dynamics to calculate the vibrational partition functions. These calculations were carried out in the GULP program,[53] using the F-SPC water model.[54] The phonon density of states calculations were performed with increasing numbers of k-points to ensure that the calculated entropy was converged. The entropies of the empty CS-II and TS-I lattices relative to that of the empty CS-I lattice are reported in Figure 8. The entropic contribution to the free energy is most stabilizing for the empty CS-I lattice. Per water molecule, the CS-II and TS-I lattices are slightly disfavored by around 0.0025 and 0.01 kcal mol^{-1}, respectively. The differences in entropic contributions for the three lattices are much smaller than the potential energy differences and do not change the stability ordering of the three structures.

The other factor that contributes to the relative thermodynamic stability of the three hydrate structures is the energy for incorporation of Br_2 molecules into the lattice. Figure 9 reports the calculated change in potential energy per molecule of Br_2 upon inclusion in the three hydrate lattices. Over the temperature range of 80−260 K our simulations indicate that it is energetically more favorable (per molecule) for Br_2 to be incorporated into the TS-I and CS-II lattices than into the CS-I lattice. This

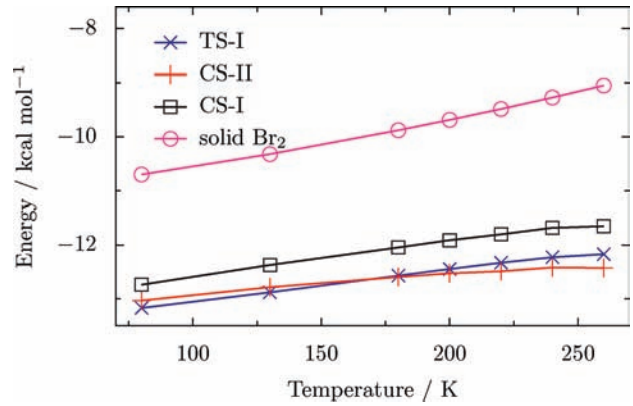

Figure 9. Stabilization energy per Br_2 molecule for inclusion in the CS-I, CS-II, and TS-I lattices. The potential energy per Br_2 in solid bromine obtained from the calorimetric measurements of ref 55 is also reported.

is consistent with the greater binding energy for Br_2 in the P and H cages than in the T cage. In all three hydrate lattices, the overall binding energies per Br_2 molecule are about 2 kcal mol^{-1} greater in magnitude than those calculated for the individual cages. By repeating the simulation with the interactions between the Br_2 molecules turned off, it is found that approximately half of this additional stabilization is due to the interaction between bromine molecules in adjacent cages. Analysis of cluster models cut out from the model crystal shows that the remainder is due to long-range interactions between a bromine molecule in one cage and the water molecules in adjacent cages.

Figure 10 plots the relative stabilization energies for incorporation of Br_2 into the CS-I, CS-II, and TS-I lattices. Although the binding energy per bromine molecule is smallest in the CS-I hydrate, the increased number of Br_2-H_2O interactions relative to the CS-II and TS-I hydrates overcomes the energy preference for the P and H cages (at least as described by the present COS-type force field). This analysis, however, ignores the fact that we are comparing systems containing different numbers of bromine molecules. Under experimental conditions the bromine hydrate crystals are generally in contact with water and residual bromine molecules that have not formed the hydrate. All temperatures considered in this study are below the freezing point of Br_2, so in order to make a more meaningful comparison, we add to the potential energies of the CS-II and TS-I hydrates the potential energies of 1204 and 238 solid-phase Br_2 molecules, respectively. This results in an equal number of Br_2 molecules in each sample. As our force field is not parametrized for the solid phase of pure Br_2, we obtain the potential energy

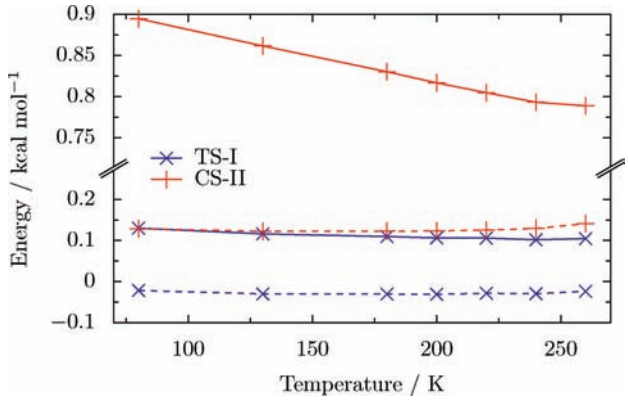

Figure 10. Relative potential energies per water molecule for including Br_2 in the CS-I, CS-II, and TS-I hydrate lattices with the CS-I lattice taken as reference. The solid lines are for the bromine:water ratio found in the fully occupied hydrates. The dashed lines report the relative energies including the potential energy of solid-phase Br_2 to make the bromine:water ratio equal for each system.

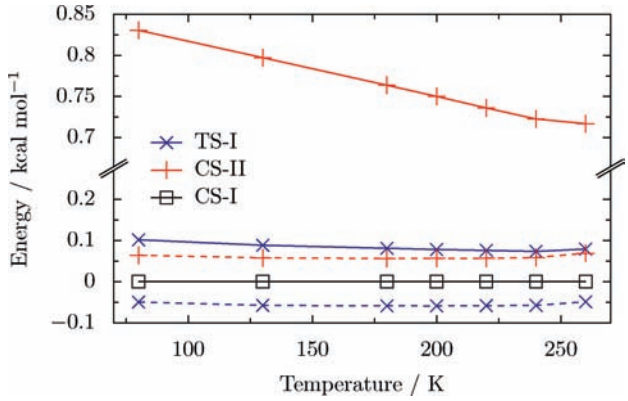

Figure 11. Potential energies per water molecule for the CS-II and TS-I hydrates relative to that of the CS-I hydrate. The solid lines are for the bromine:water ratio found in the fully occupied hydrates. The dashed lines report the relative energies including the potential energy of solid-phase Br_2 to make the bromine:water ratio equal for each system.

of the Br_2 (solid) from experimental calorimetric measurements.[55] The resulting potential energies are reported in Figure 10.

The potential energies of the CS-II and TS-II hydrates relative to that of the CS-I hydrate are reported in Figure 11. Results are reported with and without the correction using the condensed phase Br_2 contribution to make the number of Br_2 molecules commensurate. TS-I hydrate is predicted to be the energetically favored hydrate structure if the unencapsulated Br_2 is present as a solid. The energy difference between the CS-I and TS-I hydrate is very small and is of the same order of magnitude as the errors in the binding energies calculated with our force field. From the results in Table 4, we can estimate the error in our force field to be +0.5, −1.0, and −0.3 kcal mol^{-1} for incorporating a Br_2 molecule into the T, P, and H cages, respectively. Figure 12 reports total hydrate energies corrected for this deficiency in the force field. With this correction the energy separation between the CS-I and TS-I is increased, confirming that the TS-I structure is favored energetically. It is found that the CS-II hydrate is calculated to be almost isoenergetic with the CS-I hydrate, despite the fact that for the same number of water molecules, it can only encapsulate about half as many Br_2 molecules. However, because the empty lattice is the most stable and the individual encapsulation energy per

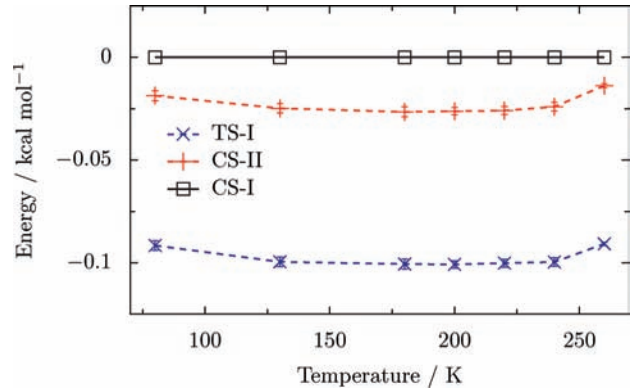

Figure 12. Potential energies per water molecule for the CS-II and TS-I bromine hydrate relative to that of the CS-I hydrate, including corrections for the binding energy difference between ab initio and model force field calculations. The potential energies of solid Br_2 have been added to the energies of the CS-II and TS-I to make the bromine:water ratio equal for each system.

Br_2 molecule most favorable in the case of the CS-II hydrate, it does seem feasible that this structure could form at low Br_2 concentrations.

In the calculations discussed above, it was assumed that all of the cages, other than the D cages, are 100% occupied. Experimentally, the larger hydrate cages are not fully occupied. Udachin et al. observe filling ratios in TS-I bromine hydrate of between 92% and 98% depending on cage type.[6] The filling ratios in CS-I and CS-II bromine hydrates are unknown.

It is also relevant to note that in the X-ray studies of Udachin et al., O_2 or N_2 molecules are incorporated in some of the D cages upon crystallization in air.[6] Because the CS-II and TS-I hydrates have a larger number of D cages than the CS-I hydrate, the incorporation of O_2 and N_2 molecules into the hydrate would act so as to stabilize the CS-II and TS-I hydrates, relative to the CS-I hydrate.

Conclusions

Molecular dynamics simulations have been used to characterize bromine hydrate crystals of CS-I, CS-II, and TS-I morphology. Direct comparison of the relative stability of the three crystals is not possible due to their different Br_2/H_2O ratios. To circumvent this problem, the energies calculated for the hydrates are combined with those of the appropriate number of solid-phase Br_2 molecules to obtain energies for systems with the same Br_2/H_2O ratios. Corrections based on the differences between the binding energies calculated ab initio and with the force field for Br_2 inside the various water cages are also applied. The net result is that the TS-I hydrate is predicted to be most stable followed by the CS-II hydrate and then by the CS-I hydrate. The preference for TS-I over CS-II and CS-I is about 0.55 and 0.75 kcal mol^{-1} per Br_2 molecule assuming full occupancy of the $5^{12}6^2$, $5^{12}6^3$ and $5^{12}6^4$ cages. Despite the relatively high energy of the CS-II hydrate, we argue that it could be formed under conditions of low Br_2 concentration. The results of the simulations are consistent with the recent experimental studies of Janda and co-workers which provided evidence for all three crystals of bromine hydrate.

Acknowledgment. We acknowledge support from the National Science Foundation. D.P.S. wishes to acknowledge the New Zealand Foundation for Research, Science and Technology for a Postdoctoral Fellowship. We also acknowledge valuable discussions with Professors Mark Rodger, Ken Janda, and Ara

Apkarian. The calculations in this work were carried out using the computer resources of the Center for Molecular and Materials Simulations at the University of Pittsburgh.

References and Notes

(1) Sloan, E. D., Jr. *Nature* **2003**, *426*, 353–359.
(2) Rondinone, A. J.; Chakoumakos, B. C.; Rawn, C. J.; Ishii, Y. *J. Phys. Chem. B* **2003**, *107*, 6046–6050.
(3) Hafemann, D. R.; Miller, S. L. *J. Phys. Chem.* **1969**, *73*, 1392–1397.
(4) Allen, K. W.; Jeffrey, G. A. *J. Chem. Phys.* **1963**, *38*, 2304–2305.
(5) Dyadin, Y. A.; Belosludov, V. R. *Comprehensive Supramolecular Chemistry*; Elsevier: Amsterdam, 1996; Vol. 6
(6) Udachin, K. A.; Enright, G. D.; Ratcliffe, C. I.; Ripmeester, J. A. *J. Am. Chem. Soc.* **1997**, *119*, 11481–11486.
(7) Dyadin, Y. A.; Bondaryuk, I. V.; Zhurko, F. V. *Inclusion Compounds: Vol. 5. Inorganic and Physical Aspects of Inclusion*; Oxford University Press: Oxford, 1991.
(8) Goldschleger, I. U.; Kerenskaya, G.; Janda, K. C.; Apkarian, V. A. *J. Phys. Chem. A* **2008**, *112*, 787–789.
(9) Janda, K. C.; Kerenskaya, G.; Goldscheleger, I. U.; Apkarian, V. A.; Fleischer, E. B. In *Proceedings of the 6th International Conference on Gas Hydrates*, 2008.
(10) Weigend, F.; Häser, M. *Theor. Chem. Acc.* **1997**, *97*, 331–340.
(11) Weigend, F.; Häser, M.; Patzelt, H.; Ahlrichs, R. *Chem. Phys. Lett.* **1998**, *294*, 143–152.
(12) Raghavachari, K.; Trucks, G. W.; Pople, J. A.; Head-Gordon, M. *Chem. Phys. Lett.* **1989**, *157*, 479–483.
(13) Hampel, C.; Peterson, K. A.; Werner, H.-J. *Chem. Phys. Lett.* **1992**, *190*, 1–12.
(14) Stevens, W. J.; Fink, W. H. *Chem. Phys. Lett.* **1987**, *139*, 15–22.
(15) Jiang, H.; Jordan, K. D.; Taylor, C. E. *J. Phys. Chem. B* **2007**, *111*, 6486–6492.
(16) Jiang, H.; Myshakin, E. M.; Jordan, K. D.; Warzinski, R. P. *J. Phys. Chem. B* **2008**, *112*, 10207–10216.
(17) Yu, H.; van Gunsteren, W. F. *J. Chem. Phys.* **2004**, *121*, 9549–9564.
(18) Peterson, K. A.; Figgen, D.; Goll, E.; Stoll, H.; Dolg, M. *J. Chem. Phys.* **2003**, *119*, 11113–11123.
(19) Barrow, R. F.; Clark, T. C.; Coxon, J. A.; Yee, K. K. *J. Mol. Spectrosc.* **1974**, *51*, 428–449.
(20) Stone, A. *J. Chem. Theory Comput.* **2005**, *1*, 1128–1132.
(21) Smith, W.; Forester, T.; Todorov, I.; Leslie, M. The DL_POLY_2.0 User Manual.
(22) Frisch, M. J.; Trucks, G. W.; Schlegel, H. B.; Scuseria, G. E.; Robb, M. A.; Cheeseman, J. R.; Montgomery Jr., J. A.; Vreven, T.; Kudin, K. N.; Burant, J. C.; Millam, J. M.; Iyengar, S. S.; Tomasi, J.; Barone, V.; Mennucci, B.; Cossi, M.; Scalmani, G.; Rega, N.; Petersson, G. A.; Nakatsuji, H.; Hada, M.; Ehara, M.; Toyota, K.; Fukuda, R.; Hasegawa, J.; Ishida, M.; Nakajima, T.; Honda, Y.; Kitao, O.; Nakai, H.; Klene, M.; Li, X.; Knox, J. E.; Hratchian, H. P.; Cross, J. B.; Adamo, C.; Jaramillo, J.; Gomperts, R.; Stratmann, R. E.; Yazyev, O.; Austin, A. J.; Cammi, R.; Pomelli, C.; Ochterski, J. W.; Ayala, P. Y.; Morokuma, K.; Voth, G. A.; Salvador, P.; Dannenberg, J. J.; Zakrzewski, V. G.; Dapprich, S.; Daniels, A. D.; Strain, M. C.; Farkas, O.; Malick, D. K.; Rabuck, A. D.; Raghavachari, K.; Foresman, J. B.; Ortiz, J. V.; Cui, Q.; Baboul, A. G.; Clifford, S.; Cioslowski, J.; Stefanov, B. B.; Liu, G.; Liashenko, A.; Piskorz, P.; Komaromi, I.; Martin, R. L.; Fox, D. J.; Keith, T.; Al-Laham, M. A.; Peng, C. Y.; Nanayakkara, A.; Challacombe, M.; Gill, P. M. W.; Johnson, B.; Chen, W.; Wong, M. W.; Gonzalez, C.; Pople, J. A. *Gaussian 03*; Gaussian, Inc.: Wallingford, CT, 2004.
(23) Werner, H.-J.; Knowles, P. J.; Lindh, R.; Manby, F. R.; Schütz, M.; Celani, P.; Korona, T.; Rauhut, G.; Amos, R. D.; Bernhardsson, A.; Berning, A.; Cooper, D. L.; Deegan, M. J. O.; Dobbyn, A. J.; Eckert, F.; Hampel, C.; Hetzer, G.; Lloyd, A. W.; McNicholas, S. J.; Meyer, W.; Mura, M. E.; Nicklass, A.; Palmieri, P.; Pitzer, R.; Schumann, U.; Stoll, H.; Stone, A. J.; Tarroni, R.; Thorsteinsson, T. *Molpro, version 2006.1, a package of ab initio programs*, 2006.
(24) Boys, S. F.; Bernardi, F. *Mol. Phys.* **1970**, *19*, 553–566.
(25) Dunning, T. H., Jr. *J. Chem. Phys.* **1989**, *90*, 1007–1023.
(26) Schmidt, M. W.; Baldridge, K. K.; Boatz, J. A.; Elbert, S. T.; Gordon, M. S.; Jensen, J. H.; Koseki, S.; Matsunaga, N.; Nguyen, K. A.; Su, S.; Windus, T. L.; Dupuis, M.; Montgomery, J. A., Jr. *J. Comput. Chem.* **1993**, *14*, 1347–1363.
(27) Buckingham, R. A. *Proc. R. Soc. London, Ser. A* **1938**, *168*, 264–283.
(28) Freitag, M. A.; Gordon, M. S.; Jensen, J. H.; Stevens, W. J. *J. Chem. Phys.* **2000**, *112*, 7300–7306.
(29) Stone, A. J. *The theory of intermolecular forces*; Oxford University Press: New York, 1996.
(30) Tang, K. T.; Toennies, J. P. *J. Chem. Phys.* **1984**, *80*, 3726–3741.
(31) Melchionna, S.; Ciccotti, G.; Holian, B. L. *Mol. Phys.* **1993**, *78*, 533–544.
(32) Hoover, W. G. *Phys. Rev. A* **1985**, *31*, 1695–1697.
(33) Berendsen, H. J. C.; Postma, J. P. M.; van Gunsteren, W. F.; DiNola, A.; Haak, J. R. *J. Chem. Phys.* **1984**, *81*, 3684–3690.
(34) Essmann, U.; Perera, L.; Berkowitz, M. L.; Darden, T.; Lee, H.; Pedersen, L. G. *J. Chem. Phys.* **1995**, *103*, 8577–8593.
(35) Miller, T. F., III.; Eleftheriou, M.; Pattnaik, P.; Ndirango, A.; Newns, D.; Martyna, G. J. *J. Chem. Phys.* **2002**, *116*, 8649–8659.
(36) Andersen, H. C. *J. Comput. Phys.* **1983**, *52*, 24–34.
(37) Buch, V.; Sandler, P.; Sadlej, J. *J. Phys. Chem. B* **1998**, *102*, 8641–8653.
(38) McMullan, R. K.; Jeffrey, G. A. *J. Chem. Phys.* **1965**, *42*, 2725–2732.
(39) Alavi, S.; Ripmeester, J. A.; Klug, D. D. *J. Chem. Phys.* **2005**, *123*, 024507.
(40) Torii, H. *J. Chem. Phys.* **2003**, *119*, 2192–2198.
(41) Legon, A. C.; Thumwood, J. M. A.; Waclawik, E. R. *Chem. Eur. J.* **2002**, *8*, 940–950.
(42) Rodger, P. M.; Stone, A. J.; Tildesley, D. J. *Chem. Phys. Lett.* **1988**, *145*, 365–370.
(43) Price, S. L.; Stone, A. J. *Mol. Phys.* **1982**, *47*, 1457–1470.
(44) Rodger, P. M.; Stone, A. J.; Tildesley, D. J. *Mol. Phys.* **1988**, *63*, 173–188.
(45) Stone, A. J.; Price, S. L. *J. Phys. Chem.* **1988**, *92*, 3325–3335.
(46) Kerenskaya, G.; Goldschleger, I. U.; Apkarian, V. A.; Fleischer, E.; Janda, K. C. *J. Phys. Chem. A* **2007**, *111*, 10969–10976.
(47) Hampel, C.; Werner, H.-J. *J. Chem. Phys.* **1996**, *104*, 6286–6297.
(48) Schütz, M. *J. Chem. Phys.* **2000**, *113*, 9986–10001.
(49) Pauling, L.; Marsh, R. E. *Proc. Natl. Acad. Sci. U.S.A.* **1952**, *38*, 112–118.
(50) Bondi, A. *J. Phys. Chem.* **1964**, *68*, 441–451.
(51) Handa, Y. P.; Tse, J. S. *J. Phys. Chem.* **1986**, *90*, 5917–5921.
(52) van der Waals, J. H.; Platteeuw, J. C. *Adv. Chem. Phys.* **1959**, *2*, 2–57.
(53) Gale, J. D.; Rohl, A. L. *Mol. Simul.* **2003**, *29*, 291–341.
(54) Tironi, I. G.; Brunne, R. M.; van Gunsteren, W. F. *Chem. Phys. Lett.* **1996**, *250*, 19–24.
(55) Hildenbrand, D. L.; Kramer, W. R.; McDonald, R. A.; Stull, D. R. *J. Am. Chem. Soc.* **1958**, *80*, 4129–4132.

JP900237J